

Measuring the magnetic-field-dependent chemical potential of a low-density three-dimensional electron gas in *n*-GaAs and extracting its magnetic susceptibility

Aditya N. Roy Choudhury* and V. Venkataraman

Department of Physics, Indian Institute of Science, Bangalore 560012, India

(Received 1 September 2015; revised manuscript received 4 November 2015; published 22 January 2016)

We report the magnetic-field-dependent shift of the electron chemical potential in bulk, *n*-type GaAs at room temperature. A transient voltage of $\sim 100 \mu\text{V}$ was measured across a Au-Al₂O₃-GaAs metal-oxide-semiconductor capacitor in a pulsed magnetic field of $\sim 6\text{T}$. Several spurious voltages larger than the signal that had plagued earlier researchers performing similar experiments were carefully eliminated. The itinerant magnetic susceptibility of GaAs is extracted from the experimentally measured data for four different doping densities, including one as low as $5 \times 10^{15} \text{cm}^{-3}$. Though the susceptibility in GaAs is dominated by Landau-Peierls diamagnetism, the experimental technique demonstrated can be a powerful tool for extracting the total free carrier magnetization of any electron system. The method is also virtually independent of the carrier concentration and is expected to work better in the nondegenerate limit. Such experiments had been successfully performed in two-dimensional electron gases at cryogenic temperatures. However, an unambiguous report on having observed this effect in any three-dimensional electron gas has been lacking. We highlight the 50 year old literature of various trials and discuss the key details of our experiment that were essential for its success. The technique can be used to unambiguously yield only the itinerant part of the magnetic susceptibility of complex materials such as magnetic semiconductors and hexaborides, and thus shed light on the origin of ferromagnetism in such systems.

DOI: [10.1103/PhysRevB.93.045208](https://doi.org/10.1103/PhysRevB.93.045208)

I. INTRODUCTION

For decades, itinerant electron magnetism in solids has been a widely researched topic (see, for example, Ref. [1]). Interest in this topic has recently increased owing to the advent of certain man-made complex material systems and the field of spintronics, where scientists have been interested in knowing what part of a solid's total magnetization originates from its itinerant carriers. The majority of the scientific focus is on the ferromagnetism of the free electron gas in doped semiconductors.

The possibility of itinerant electron ferromagnetism in diluted magnetic semiconductors (DMSs) [2,3] has practical implications for the realization of semiconductor spintronic devices [4,5]. Reports of ferromagnetism in DMS materials such as GaMnAs exist [6,7], but there are conflicting opinions regarding its origin [8]; the role of localized magnetic moments of the dopant atoms [7] or the magnetic interactions in the precipitates of dopants [9,10], or that of foreign impurities such as Fe incorporated during sample preparation [8] cannot be ruled out. Unusual magnetization behavior has also been theoretically predicted in DMS materials in the low carrier density regime [11].

There is also a fundamental scientific interest in the magnetic states of a low-density, interacting electron gas [12]. A century ago, the possibility of a first-order phase transition of the free electron gas to a spin polarized ground state, at sufficiently low densities, was pointed out by Bloch by using a Hartree-Fock model [13]. Subsequently, Stoner theoretically predicted a second-order phase transition [14,15]. One should refer to Ref. [12] for a comprehensive overview of the subject. In the last decade, a new class of doped semiconductors, the hexaborides [8,16], has attracted much attention since the first

report of room temperature ferromagnetism in $1 \times 10^{21} \text{cm}^{-3}$ La-doped CeB₆ [16]. It was suggested at that time [17] that the long sought after Bloch ferromagnetism was possibly detected. However, subsequent reports by other groups proposed other possibilities for the observed magnetic behavior [8], including those of excitonic origins [18] as well as those originating from small amounts of unintentional ferromagnetic impurities in the samples [8]. At present, the situation in the hexaborides remains inconclusive [8].

Meanwhile, in the independent electron picture, itinerant electron magnetism consists of only an orbital (Landau diamagnetic) and a spin (Pauli paramagnetic) contribution [1,19]. In typical metals, the electron density is sufficiently high to let itinerant magnetism dominate. In the case of doped semiconductors, however, itinerant magnetism is much smaller compared to that originating from localized moments. The main experimental challenge is to disentangle this small contribution from the total magnetization/susceptibility that is otherwise measured by instruments such as a vibrating sample magnetometer (VSM), a superconducting quantum interference device (SQUID), or a Faraday balance. One approach is to systematically measure the susceptibility for different doping levels and subtract the measured susceptibility of the undoped sample from them. This is possible for high carrier densities, but becomes progressively error prone as the carrier density is reduced. This approach is discussed in more detail in Sec. III B.

From the above discussion, it is apparent that there is a need for an experimental technique that can directly measure the magnetization/magnetic susceptibility of itinerant carriers, especially in the presence of larger background contributions from the host lattice, dopants, unintentional magnetic impurities, etc. It has been known for some time now that a measurement of the chemical potential (μ) of the electron gas as a function of magnetic field (B) would serve that purpose. The chemical potential is related to the magnetization (M)

*aditya@physics.iisc.ernet.in

by one of Maxwell's celebrated thermodynamic relations, $M = -N(\partial\mu/\partial B)_{N,T,P}$, and therefore to the magnetic susceptibility by $\chi = -N(\partial^2\mu/\partial B^2)_{N,T,P}$, where N is the carrier concentration, T is the temperature, and P is the pressure.

Magnetization has been calculated from such chemical potential changes before, however, only for two-dimensional electron gases (2DEGs) at cryogenic temperatures [20–22]. The shift in electron chemical potential for bulk, doped semiconductors is very small, of the order of a few hundreds of μeV at low temperatures, even if the field is varied by a few tesla (see Sec. V A). It is challenging to measure such small shifts as they are easily overcome by spurious effects. It is even more challenging to measure these at room temperature.

In this paper, we measure the shift in the chemical potential of a low-density electron gas in n -type, bulk GaAs at room temperature in fields up to ~ 6 T. Improvements in electronics, signal processing, as well as careful attention to the experimental layout has enabled the observation of clear signals from the itinerant electrons at densities as low as $5 \times 10^{15} \text{ cm}^{-3}$, circumventing the spurious effects that had plagued earlier researchers. More than 200 experiments with pulses of 6 T field, in different orientations, and on a variety of doped GaAs samples, as well as control samples of Si and other materials, have been analyzed. The magnetic susceptibilities derived from these measurements agree reasonably well with theoretical calculations, assuming independent electrons, in n -GaAs.

II. BASIC PRINCIPLE

Consider a piece of doped semiconductor electrically isolated from a metallic reference electrode. The difference in the electron chemical potentials between the two systems is known as the contact potential. If the two systems are now electrically connected, electrons are exchanged until the resulting electrostatic potential fully compensates for the contact potential, i.e., until the electrochemical potentials of the two systems become equal and equilibrium is achieved. By measuring the transient current and the capacitance between the two systems, the charge transfer and the developed electrostatic potential can be determined, which directly gives the contact potential. The duration of this transient current depends on the capacitance and the resistance of the circuit. For ease of measurement, a steady state periodic nonequilibrium current can be generated by continuously oscillating the distance between the two systems, thus varying the capacitance periodically. This is the basis of Kelvin's method of measuring contact potentials [23].

The electron chemical potential μ depends on magnetic field B owing to the field dependence of the electron density of states (see Sec. V A). To find the free carrier magnetization M , one could perform the Kelvin method in magnetic fields. When B is switched on, any change in μ of the doped semiconductor (with respect to that of a metallic reservoir), where the two systems are electrically connected, is quickly compensated by transient currents. As a consequence, a magnetic-field-dependent built-in electric potential $V_{\text{bi}}(B)$ develops across the capacitor. However, there is no signal in equilibrium for steady fields. The magnetic fields required to significantly alter the μ are large (a few tesla) and hence it is difficult to measure steady

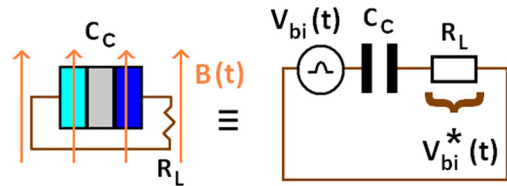


FIG. 1. Electrical equivalent circuit of the MOS capacitor sample in a time-varying magnetic field. V_{bi} can be modeled as a time-varying voltage source in series with the MOS capacitance C_C and the externally put resistor R_L . The voltage drop to be experimentally measured is $V_{\text{bi}}^* < V_{\text{bi}}$. The circuit is a classic example of a first-order, RC high pass filter (HPF).

currents, as in the Kelvin method, using continuous oscillating fields. On the other hand, it is possible to generate single large field transient pulses using well established pulsed magnet techniques [24]. This is the basic idea behind our experiment.

The actual sample is a metal-oxide-semiconductor (MOS) capacitor consisting of a doped semiconductor (n -type GaAs) and a metallic reservoir (Au gate metal) separated by a thin dielectric oxide (Al_2O_3) layer. The capacitance is C_C . During the magnetic field pulse, a transient current flows through the resistor R_L that is externally connected to the MOS capacitor. The magnitude of this current can be measured as a voltage drop across R_L . The electrical equivalent circuit of the arrangement is depicted in Fig. 1. Once the magnetic field pulse is over, the current decays to zero after a few τ 's, where $\tau = R_L C_C$ is the time constant of the RC circuit. The voltage V_{bi}^* that is dropped across the resistor R_L is smaller in magnitude than V_{bi} owing to the finiteness of τ . Both the B and the V_{bi}^* transients are simultaneously recorded and analyzed to obtain the B dependence of the semiconductor's μ [25].

III. HISTORICAL REVIEW

A. Field dependence of the chemical potential

Though magnetic-field-induced oscillations of μ have been detected before for 2DEGs at cryogenic temperatures [26–32], an experimental detection of μ 's magnetic field dependence in any three-dimensional (3D) system has eluded experimentalists for decades. Over the last 50 years, the experiment has been tried in ferromagnetic metals (Fe [33] and Ni [22,34]), nonferromagnetic metals (Pb [35], Zn [36], and Be [37]), semimetals (Bi [29,38] and Sb [39]), and superconductors (Yttrium barium copper oxide) [22,40]. None of these attempts has yielded any positive and reproducible result [41–43].

The experiment has been tried in pulsed magnets before [38,39]. In fact, when the idea was first proposed in 1957 [44] and 1963 [45], the authors suggested the use of pulsed magnets [45] so that the experiment could be performed even at noncryogenic temperatures. Measuring small voltages, with high accuracy and precision, in a pulsed magnetic field is a tough task owing mainly to the presence of a spurious pickup voltage that gets inductively induced in the sample wiring following Faraday's law of electromagnetic induction. Unless this effect is considerably reduced, performing this experiment in a high time-varying magnetic field is futile. Previously, this had made experimentalists avoid pulsed magnets [35]. In

fact, Ref. [38] is the only instance where this experiment was performed in a pulsed field and the issue of the pickup was also properly addressed.

Another spurious effect connected with this experiment was unveiled in 1970 [43] and, after its discovery, many apparent claims [35,36,38,39] of previously having successfully detected $\mu(B)$ in 3D materials were further scrutinized. As the magnetic field changes with time, it gives rise to an eddy current in the sample. This current and the field then gives rise to an unwanted Hall voltage [42,43] which was often seen to be greater in magnitude than the expected signal [35,36]. In this work, the magnitude of this spurious effect was experimentally seen to depend on the direction of the applied magnetic field, making the measured signal across the resistor R_L dependent on the field direction. Details follow in Sec. VIII. Though Ref. [43] says that the previous works in Bi [38] and Sb [39] may have been authentic, no mention is made of the spurious Hall voltage in either of these two papers.

B. Itinerant magnetism in bulk semiconductors

On searching the literature, one finds a lot of work, both experimental [46,47] and theoretical [48–54], that has gone into the magnetism of bulk (nonferromagnetic) semiconductors. The following is a glimpse of the huge volume of literature available on the subject: Refs. [55–60] on Ge, Refs. [61–64] on Si, Refs. [65,66] on InSb, and Refs. [67–70] on GaAs.

One of the earliest works that expressed the total magnetic susceptibility of a semiconductor in terms of the individual contributions from its lattice, free carriers, and dopants/impurities was Ref. [71]. Since then much effort has gone into trying to experimentally segregate each of these three contributions from the other two. For extracting the free carrier term, experimentalists had measured the magnetic susceptibilities of a highly doped sample and a low-doped one and then had subtracted the latter from the former (see Ref. [70] for GaAs, Refs. [55,56,59] for Ge, Refs. [65,66] for InSb, and Refs. [61,72] for Si).

However, this procedure experimentally suffers from noisy data, especially at low carrier concentrations as the magnetic susceptibilities of intrinsic/low-doped semiconductors are too low to be measured accurately and precisely within the sensitivity of the instruments available. For example, the minimum electron concentration, for which such an experiment was successful, was $\sim 10^{17} \text{ cm}^{-3}$ for n -type GaAs (SQUID [70]) and $\sim 10^{16} \text{ cm}^{-3}$ for n -type Ge (Faraday balance [55]), where even the sample volumes (single crystal cubes of $\sim 5 \text{ mm}$ edge length) were more than an order of magnitude greater than what we have used in this paper. Instead, for the technique we demonstrate in this paper, the smaller the carrier concentration, the higher is the signal one should get. Calculations show that the expected V_{bi} is independent of the carrier concentration in the nondegenerate limit (see Sec. V).

IV. THE EXPERIMENTAL SETUP

A tabletop bank of electrolytic capacitors, consisting of nine numbers of 450 V/4.7 mF and five numbers of 450 V/2.2 mF capacitors in parallel, is connected to a thyristor (Semikron SKT 300/16E) and a magnet coil in series. The bank is charged

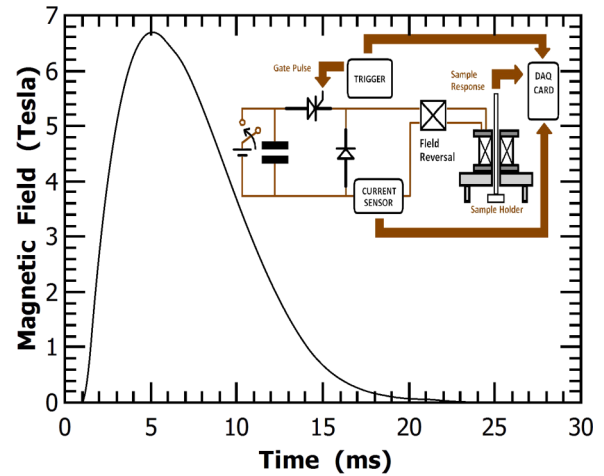


FIG. 2. The magnetic field pulse as experimentally measured. The DAQ card records data from 1.024 ms before the pulse starts. The inset shows the schematic of the pulsed magnet setup.

slowly by a dc power supply and then discharged into the magnet coil by the thyristor. A crowbar diode (Semikron SKR 320/16) is connected antiparallel across the magnet for freewheeling of the large current; the current is diverted through the diode when the underdamped discharge tries to invert the voltage polarity of the capacitor bank. A monostable multivibrator [73] simultaneously triggers both the thyristor and the data acquisition (DAQ) card (PCI-DAS 4020/12). The high current part of the circuit was well isolated from the low level data acquisition part by a couple of pulse isolation transformers [73]. The current sensor (LEM LF 2005-S) directly measures the magnet current and gives a proportionate voltage output to the DAQ card, thereby measuring the magnetic field. The direction of the field can be changed, from one pulsing to another, using the changeover switch. The 12-bit DAQ card measures the output voltage at a sampling rate of 1 MHz. Figure 2 shows the magnetic field pulse as well as the full setup.

The dB/dt was seen to be greater than 1.5 kT/s. Preliminary measurements reveal a spurious pickup voltage (which the reader has been introduced to in Sec. III A) of $\sim 60 \text{ mV}$ that gets induced in the sample wirings even when no sample is connected. However, the pickup changes sign with a reversal in the magnetic field direction, unlike the sample signal originating from $\mu(B)$. This enables us to perform pickup cancellation by algebraically adding two separate measurements that differ only in the direction of the applied field. All data processing was done in MATLAB. Even such a step proves to be insufficient to detect signals as low as $100 \mu\text{V}$ and hence we decide to pass the sample response through an amplifier first to increase the signal-to-pickup ratio at its output. Such a step can only work when the amplifier sits right next to the sample inside the magnet bore rather than outside the magnetic field. We build a simple, single stage, noninverting operational amplifier (op-amp) circuit with the instrumentation amplifier chip INA121 on a printed circuit board (PCB) using all surface mount (SMD) components. An amp gain of ~ 200 was put. The amp gain was verified to be unaffected in the high magnetic field environment. The setup

eventually gave a stable background of $\pm 20 \mu\text{V}$. Thus any sample response exceeding $20 \mu\text{V}$ could be measured in our setup. More than 90% pulse-to-pulse data reproducibility was achieved with a pickup cancellation accuracy of $> 99\%$. The magnetic field pulse was verified to be reproducible within 600 G. Further details about the setup, including the PCB amplifier details and details regarding sample mounting and soldering, have been given in the Supplemental Material [74].

V. ESTIMATED SIGNAL

A. Estimating $V_{\text{bi}}(B)$

For a bulk semiconductor subject to an external magnetic field, the density of electronic states, with the spin splitting taken into account, can be expressed as [75]

$$DOS_B(E) = \frac{qB}{h} \left(\frac{2m^*}{\hbar^2} \right)^{\frac{1}{2}} \left[\sum_{n=0}^{\nu} \left(E + \frac{g^* \mu_B B}{2} - E_n \right)^{-\frac{1}{2}} + \sum_{n=0}^{\nu} \left(E - \frac{g^* \mu_B B}{2} - E_n \right)^{-\frac{1}{2}} \right]. \quad (1)$$

Here, $E_n = (n + \frac{1}{2})\hbar\omega_C$ are the Landau levels, where $n = 0, 1, \dots, \nu$; ν is the largest possible integer for which $(E - E_n) > 0$ for a given E ; g^* is the electron effective g factor and μ_B is the Bohr magneton.

We have ignored any effects from disorder broadening of Landau levels. Such a step is justified if the thermal energy $k_B T$ exceeds the broadening parameter $\Gamma = \frac{\hbar}{\tau_s}$ [76,77]. $\tau_s = \frac{\mu_e m^*}{q}$ is the mean free time for electron scattering, m^* is the effective electron mass, and k_B is the Boltzmann constant. Assuming an electron mobility $\mu_e \sim 1800 \text{ cm}^2 \text{ V}^{-1} \text{ s}^{-1}$ (the least possible electron mobility for the GaAs sample of highest doping that we have used, confirmed from the wafer manufacturer's data sheet), one derives a maximum possible broadening of $\Gamma \sim 10 \text{ meV}$, which is still less than the thermal energy at 300 K ($\sim 26 \text{ meV}$).

Irrespective of the magnetic field B , the electronic concentration N remains fixed for a given sample,

$$N = \int_0^{\infty} DOS_B(E) f_B(E) dE, \quad (2)$$

where f_B is the magnetic-field-dependent Fermi-Dirac distribution, $f_B(E) = [1 + \exp\{\frac{E - \mu(B)}{k_B T}\}]^{-1}$.

Equation (2) can be analytically solved for $\mu(B)$ in the nondegenerate limit; this is partly derived in Ref. [75]:

$$\begin{aligned} \mu(B) &= k_B T \ln \left[\frac{\sinh(\theta)}{\theta \cosh(\alpha)} \right] \\ &= k_B T \left[\ln \left\{ \frac{\sinh(\theta)}{\theta} \right\} - \ln \{ \text{sech}(\alpha) \} \right]. \end{aligned} \quad (3)$$

In Eq. (3), the θ term is associated with Landau diamagnetism and the α term with Pauli paramagnetism. $\theta = \frac{\hbar\omega_C}{2k_B T}$ and $\alpha = \frac{g^* \mu_B B}{2k_B T}$. The field-independent offset owing to $\mu(0)$, the electron chemical potential at $B = 0$, has been ignored by us. Note that the derived $\mu(B)$ is independent of carrier concentration. However, when the nondegenerate approximation does not hold, $\mu(B)$, at a given B , decreases with increasing carrier

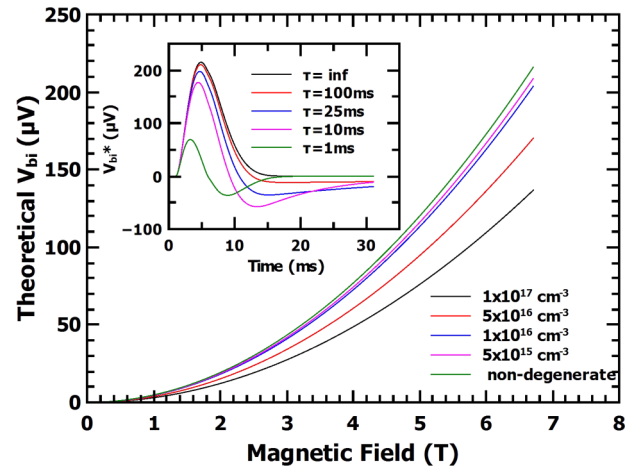


FIG. 3. The magnetic field dependence of the electron chemical potential in n -type GaAs at room temperature, for various doping densities, as estimated numerically in MATLAB. The inset shows an estimate of the theoretical V_{bi}^* that the setup should measure across the load resistor R_L (referring to Fig. 1). The smaller the time constant τ ($= R_L C_C$), the smaller is V_{bi}^* . $V_{\text{bi}}^* = V_{\text{bi}}$, for infinite τ . For the inset, we have assumed $N_D = 5 \times 10^{15} \text{ cm}^{-3}$.

concentration; this has been verified by numerical estimations done in MATLAB.

Figure 3 shows the graphical behavior of $\mu(B)$, for various doping densities, estimated through such numerical simulations. Further details of these calculations can be accessed in the Supplemental Material [74].

It was also verified in MATLAB's curve fitting toolbox that each of the plots has a $\sim B^2$ field dependence. Thus, the weak-field approximation ($\theta < 1, \alpha < 1$) was verified to be valid in our case (we have, for $B = 7 \text{ T}$ and $T = 300 \text{ K}$ in GaAs, $\hbar\omega_C \sim \frac{k_B T}{2}$). The curve for the nondegenerate case, as shown in Fig. 3, was calculated analytically from Eq. (3).

Analysis also shows that, for n -type GaAs, the diamagnetic contribution dominates $\mu(B)$. The Pauli paramagnetism is negligibly small. This means one would not get a very different estimate if the spin splitting of the Landau levels is neglected for n -GaAs.

B. Difference between V_{bi}^* and V_{bi}

The inset of Fig. 3 shows the estimated signal $V_{\text{bi}}^*(t)$ for a given GaAs doping density (i.e., for a given V_{bi}) and for various time constants τ ($= R_L C_C$). The reader is referred back to Fig. 1. The temporal shapes of $V_{\text{bi}}^*(t)$ have been derived from that of the high magnetic field pulse $B(t)$ shown in Fig. 2. We use a pulsed magnet with a pulse width of $\sim 20 \text{ ms}$ and a peak field of $\sim 6.7 \text{ T}$. Also note from Fig. 2 that the rising part of the magnetic field pulse is sinusoidal in nature with a rise time of $\tau_{\Delta B} \sim 4 \text{ ms}$.

Referring to Fig. 1, for the case of $\tau_{\Delta B} \ll R_L C_C$, $V_{\text{bi}}^* \approx V_{\text{bi}}$ as then the frequency of the V_{bi} pulse is beyond the cutoff frequency $\approx 1/(R_L C_C)$ of the HPF. However, for cases such as ours where $\tau_{\Delta B} \approx R_L C_C$, both the real (resistive) and the imaginary (capacitive) parts of the transient current flowing through R_L should be taken into account. From a simple

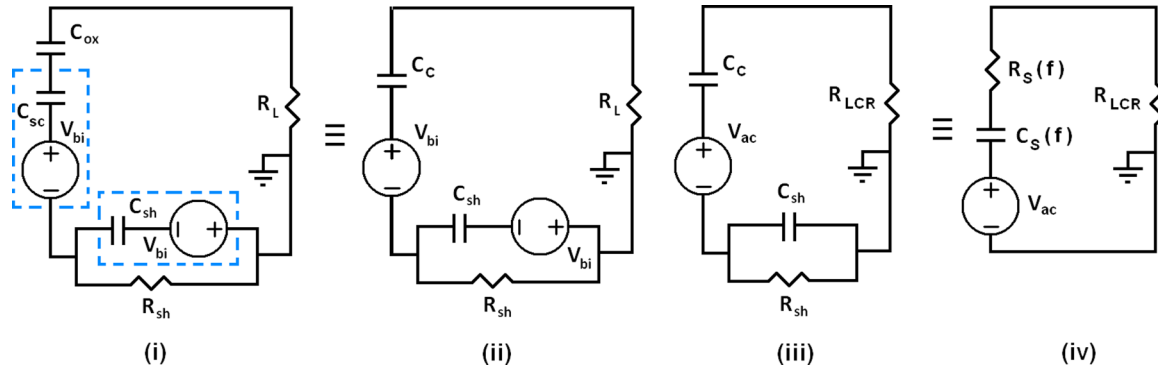


FIG. 4. Equivalent circuits of the MOS capacitor assuming a Schottky back contact. (i) and (ii) depict equivalent circuits in a magnetic field. Also, an additional V_{bi} in series with the Schottky capacitance C_{sh} , is worthy of note; it originates from the same reasoning as the V_{bi} in series with C_{sc} does. (iii) and (iv) depict the same equivalent circuit when the MOS capacitor is excited by an electrical voltage source V_{ac} instead of V_{bi} . The Schottky element renders the C_s, R_s frequency-dependent.

time-domain analysis of this HPF, one arrives at

$$V_{bi}^*(t) = V_{bi}(t) - \frac{Q_M(t)}{C_C}, \quad (4)$$

where $Q_M(t)$ is the charge stored in the gate metal at time t ,

$$Q_M(t) = \left[\frac{\exp\left(-\frac{t}{R_L C_C}\right) \left\{ \int V_{bi}(t) \exp\left(\frac{t}{R_L C_C}\right) dt \right\}}{R_L} \right]. \quad (5)$$

Thus Eqs. (4) and (5) help one to estimate the theoretical V_{bi}^* , using the theoretically estimated V_{bi} from Fig. 3, for a given GaAs doping density. Results are shown in the inset of Fig. 3. C_C can be measured experimentally for a given sample. In practice, C_C is the combined capacitance of the oxide capacitance C_{ox} and the semiconductor capacitance C_{sc} in series. R_L is put externally and so its value can be independently fixed. We put $R_L = 10 \text{ M}\Omega$.

A thorough discussion of $V_{bi}^*(B)$ is important as that is what one experimentally measures instead of $V_{bi}(B)$. All calculations of V_{bi}^* here assume an ohmic back contact to the GaAs.

VI. SAMPLE FABRICATION

GaAs wafers, with five different doping densities, were bought from MTI, USA [$N_D \sim 1 \times 10^{17} \text{ cm}^{-3}$ (denoted as type S1) and $N_D \sim 5 \times 10^{16} \text{ cm}^{-3}$ (type S2)] and from CMK, Slovakia [$N_D \sim 1 \times 10^{16} \text{ cm}^{-3}$ (type S3), $N_D \sim 5 \times 10^{15} \text{ cm}^{-3}$ (type S4), and $N_D \sim 2 \times 10^{15} \text{ cm}^{-3}$ (type S5)]. The wafers were cut into small ($\sim 3 \text{ mm} \times 3 \text{ mm}$) square pieces and were RCA cleaned. The samples were ultrasonicated successively in Isopropyl alcohol, acetone, and methanol for 5 min each and then in de-ionized (DI) water for 2 min. This was followed by a 5 min dip in 1 : 1(37%)HCl : H₂O to strip off any native oxide layer [78]. Then they were rinsed in DI water for ~ 30 –60 s. Next, atomic layer deposition (ALD) of Al₂O₃ was performed in a thermal ALD reactor (TFS-200, Beneq Oy, Finland) at $T = 250^\circ\text{C}$. A typical thickness of the insulator deposited was $\sim 20 \text{ nm}$, as verified later by ellipsometry. The back surface was roughened using a diamond cutter tip and 200 nm thick Au dots were deposited on either side (i.e., as the back contact as well as the gate metal) by e -beam evaporation through a pair of shadow masks (this shadow

mask pair was “aligned” to reduce spurious Hall voltage in the measurements, as discussed in Sec. VIII). The dots are 1 mm in diameter. No annealing was done in any step. More on sample fabrication follows in the Supplemental Material [74].

The absence of any annealing hinders the formation of ohmic back contacts and we have Schottky back contacts instead on our GaAs samples. We tried to anneal the samples, as annealing is an important step in the fabrication of such MOS capacitors; virtually all ohmic contact formation methods on GaAs require annealing [79]. However, any heat treatment was either seen to reduce the capacitance to values lower than 1 nF or was seen to increase the dc leakage (thus reducing our $R_L C_C$). We tried using Pd/Ge ohmic contacts even by performing a rapid thermal anneal [80,81], but the mentioned problems associated with annealing persisted. So we decided to stick to Schottky back contacts.

Schottky back contacts complicate the estimate of V_{bi}^* and one could no longer consider Fig. 1 as the equivalent circuit or Eq. (4) to be valid. More details on how to analyze and characterize the equivalent circuit and V_{bi}^* in the presence of Schottky back contacts, are given in Sec. VII.

VII. EXPERIMENTAL RESULTS

A. Electrical characterization

The equivalent circuit for metal-semiconductor Schottky contacts can be found in the literature (for example, see Refs. [82–84]). The updated equivalent circuit of the MOS capacitor in a pulsed magnetic field, this time with the Schottky back contact, is depicted in Fig. 4(ii).

Here, C_{sh} and R_{sh} are the Schottky capacitance and resistance, respectively. It is interesting to note the presence of V_{bi} in series with C_{sh} as well. Figure 4(i) justifies the existence of this extra back contact V_{bi} by comparing C_{sh} with C_{sc} . Figure 4(iii) shows the sample equivalent circuit when it is instead connected to an impedance analyzer (LCR meter, HIOKI 3532-50, for our case) outside the magnetic field. In this case the stimulating voltage is caused by an electrical ac voltage source V_{ac} instead of the pulsed V_{bi} driven by the magnetic field. Unlike the magnetic field, an electrical source does not get access to the Schottky back contact separately and so an analogous back contact V_{ac} is absent in Fig. 4(iii).

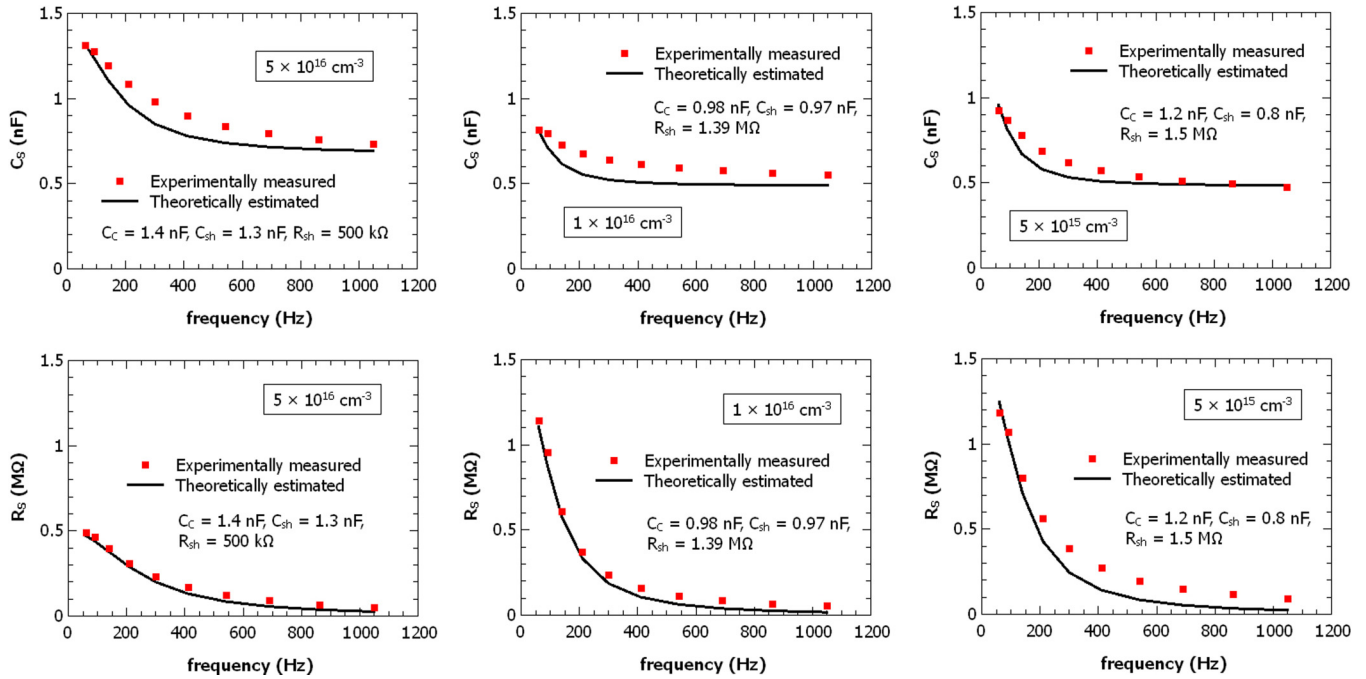


FIG. 5. Frequency-dependent C_S and R_S values of the MOS capacitor samples measured by the *LCR* meter outside any magnetic field. These values are fitted to Eqs. (6) and (7) to obtain possible values of C_C , C_{sh} , and R_{sh} for each sample. The curve fittings are done in MATLAB. Here, we show results for the three lower doped samples.

The *LCR* meter detects the total current, having both real and imaginary components, flowing through R_{LCR} . Figure 4(iv) shows the C_S, R_S mode in which the *LCR* meter takes data, where C_S and R_S are now dependent on the frequency f of V_{ac} [Eqs. (6) and (7); $\omega = 2\pi f$],

$$\frac{1}{C_S} = \frac{1}{C_C} + \frac{\omega^2 C_{sh} R_{sh}^2}{(1 + \omega^2 C_{sh}^2 R_{sh}^2)}, \quad (6)$$

$$R_S = R_{sh} \left(\frac{1}{1 + \omega^2 C_{sh}^2 R_{sh}^2} \right). \quad (7)$$

The impedance of the MOS capacitor samples are measured in the *LCR* meter within a frequency range of 60 Hz to 1 kHz. Figure 2 confirms the magnetic field pulse being composed of frequencies well below the 1 kHz limit. The results are shown in Fig. 5 and are fitted to Eqs. (6) and (7) to find the parameters C_C , C_{sh} , and R_{sh} for each sample.

For the sample with a doping density of $1 \times 10^{17} \text{ cm}^{-3}$ we could only measure the C_S, R_S at $f = 60 \text{ Hz}$ (as $C_S = 2.6 \text{ nF}$ and $R_S = 60 \text{ k}\Omega$). Before the frequency-dependent study could be done, unfortunately, the gate contact came off. For this sample, to compare the magnetic field signal with a theoretical estimate, we crudely assume $C_C = C_{sh} = 2.6 \text{ nF}$ and $R_{sh} = R_S = 60 \text{ k}\Omega$. Though crude, such assumptions can be justified using Eqs. (6) and (7). The range of the fitted C_C , C_{sh} , and R_{sh} values obtained from Fig. 5 can be theoretically justified (see the Supplemental Material [74]).

B. Magnetic field signals

We show the experimentally measured signals [85] in Fig. 6 for all the four samples, with each of the samples oriented with their planes parallel to the magnetic field direction. When kept

perpendicular, the measured signals are quite different, and this has been tested several times for each sample—with the signal obtained for a given sample, and a given orientation angle being very reproducible from one measurement to another. The reason behind such an apparent anomaly is the spurious Hall voltage, an additional, unwanted voltage which gets added to V_{bi}^* and is only generated when the sample is not parallelly oriented to the magnetic field. This spurious effect has been explained and verified in Sec. VIII.

The theoretically estimated V_{bi}^* s, also shown in Fig. 6, are generated using LTSPICE simulations taking Fig. 4(ii) as the equivalent circuit in the magnetic field, and using the very same C_C , C_{sh} , and R_{sh} values obtained from MATLAB curve fittings in Fig. 5 for each sample. Note that the V_{bi} used in such LTSPICE simulations is different for each sample (see Fig. 3). It is also assumed in the LTSPICE simulations that none among C_C , C_{sh} , and R_{sh} changes when subject to a magnetic field.

VIII. THE SPURIOUS HALL VOLTAGE

The primary reason why μ vs B could not be unambiguously detected before, for a 3D material, is a spurious Hall voltage that arises from the combination of the time-varying magnetic field and the eddy current that it induces in the sample [42,43]. This Hall voltage cannot be canceled as the pickup (we explain why later), and hence always adds to the sample signal unless minimized with care. Thus, it would be unwise to report any μ vs B observations for a 3D material without explaining how the measurements were protected from getting affected by this spurious effect. Note that this spurious voltage is present even without any deposited insulator on the semiconductor sample. Figure 7's inset schematically shows how this Hall voltage gets generated.

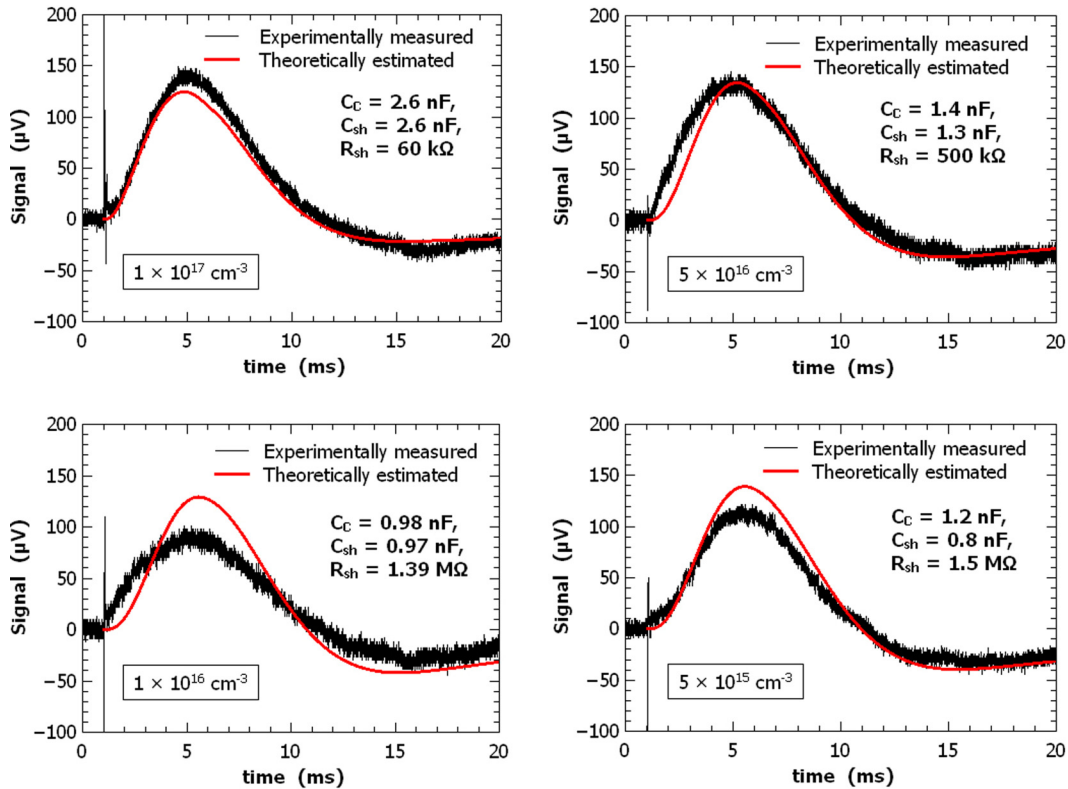


FIG. 6. Measured signals (i.e., experimentally measured V_{bi}^*) in parallel sample configuration for different doping densities S1–S4, along with their corresponding theoretical estimates. The estimated curves were obtained from LTSPICE simulations with the samples' equivalent circuit as described in Fig. 4(ii) with the C_C , C_{sh} , and R_{sh} values obtained from curve fittings to the frequency-dependent impedances for each sample (Fig. 5).

Consider two contacts made to the semiconductor—one at the center “C” and another at the edge “E.” The contacts may be made on the same surface (as shown in Fig. 7’s inset) or on opposite surfaces. Assuming $d \ll w$, it should not make any difference whether or not the contacts are on the same surface. A time-varying magnetic field in the Z direction induces an eddy current in the sample, as shown in the schematic. This eddy current in the presence of the magnetic field gives rise to a Hall voltage between the two contacts C and E. Because the sample here is n type, the potential at E will be positive with respect to C.

Figure 7 shows the shape of the Hall voltage in our setup, plotted against time, when compared to that of the magnetic field, estimated V_{bi} , or the pickup. The value of this spurious Hall voltage can be estimated as follows. Consider w' to be the distance between the two contacts C and E, and w and d to be the dimensions of the bulk, square sample (as shown in Fig. 7’s inset). Then, one has

$$V_{Hall} = w' v B, \quad (8)$$

where v is the velocity of the electrons.

Let the eddy current I_{eddy} face a cross-sectional area A_{eddy} as it flows through the bulk sample. Then, $I_{eddy} = NqA_{eddy}v$. Also, one arrives at $I_{eddy} = (V_{pickup}/R_{eddy})$, where V_{pickup} is the pickup voltage induced in the sample owing to the changing magnetic field and R_{eddy} is the resistance the eddy current faces while flowing through the sample. From Faraday’s law of electromagnetic induction, $V_{pickup} = (A_{loop} \frac{dB}{dt})$, where A_{loop} is

the sample cross-sectional area the magnetic field cuts through, perpendicularly. Also, a simple estimate of the resistance would be $R_{eddy} = \frac{\rho_s L_{loop}}{A_{eddy}}$, where ρ_s is the resistivity of the semiconductor and L_{loop} is a measure of the length of the eddy current’s circular flow path. Rough estimates of L_{loop} and A_{loop} would be $L_{loop} \sim \pi w'$ and $A_{loop} = \frac{\pi w'^2}{4}$.

All this leads to a simple expression for the Hall voltage,

$$V_{Hall} = \frac{w'^2 B}{4Nq\rho_s} \frac{dB}{dt}. \quad (9)$$

Finally, taking μ_e as the electron mobility for the given doping of the semiconductor, and at the given temperature, we get

$$V_{Hall} = \frac{w'^2 \mu_e}{4} B \frac{dB}{dt}. \quad (10)$$

Equation (10) derived here is similar to the expression of the Hall voltage that is stated in Refs. [42,43], where it was derived for a cylindrical sample geometry.

Now, though this spurious Hall voltage is dependent on the orientation of the sample (the above derivation is done assuming that $\phi = \pi/2$, where ϕ is the angle made by the sample plane with respect to the field direction), one interesting point to note here is, unlike the orientation dependence of a conventional Hall voltage which goes as $\sim \sin \phi$, here one has a $\sim \sin^2 \phi$ dependence instead. One additional factor of $\sin \phi$ comes from the $\frac{dB}{dt}$ term. Such a peculiar property of this Hall

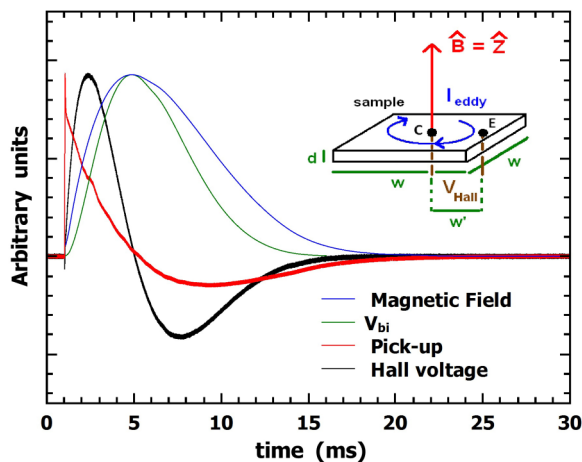


FIG. 7. Temporal shapes of various voltages and how they differ from each other. The magnetic field (B) is obtained from the current measured by the current sensor. The pickup (dB/dt) is the spurious voltage measured at the amplifier's output even when no sample is connected. The Hall voltage ($B \times dB/dt$) can be obtained by subtracting the measured “parallel signal” from the measured “perpendicular signal” as described in text. V_{bi} (which goes as B^2) is theoretically calculated. The magnetic field, the pickup, and the Hall voltage have been scaled here to match V_{bi} in magnitude. The scaling is undertaken primarily to compare the temporal shapes of all the different curves. Inset: Sample schematic, without any insulator, illustrating the generation of the spurious Hall voltage.

voltage makes it impossible to be canceled by just changing the magnetic field direction in a second measurement—the procedure that we otherwise follow to cancel out the pickup. This makes us try and minimize this spurious voltage by other methods available, such as keeping the sample parallel to the magnetic field (i.e., minimizing ϕ itself).

The presence of an additionally deposited insulator on the substrate does not affect the Hall voltage much, except that it can at most decrease the Hall voltage's magnitude by a small amount (as the Hall voltage gets passed through the HPF). For our samples, the two contacts—one to the semiconductor and the other to the gate—are deposited with utmost care so that there is maximum alignment between them; this minimizes w' in the Hall voltage expression above. Hence, we deposit the metal contacts through an aligned pair of shadow masks which give us “central contacts” on both sample surfaces.

In Fig. 7, the pickup and the spurious Hall voltages are scaled to the V_{bi} estimated from n -GaAs ($\sim 200 \mu\text{V}$). The actual pickup and the Hall voltage are larger by $90\times$ and $0.5 - 10\times$ (randomly varying from one sample to another), respectively. The GaAs doping density considered for estimating the V_{bi} in Fig. 7 is $N_D \sim 5 \times 10^{15} \text{ cm}^{-3}$ (i.e., S4). The magnitude of the Hall voltage can be minimized or maximized by suitably orienting the sample in the magnetic field. One may also have a “negative Hall voltage” which would then correspond to the given Hall shape mirrored against the time axis. The mentioned direction of the Hall voltage solely depends on the relative alignment of the gate and back contacts.

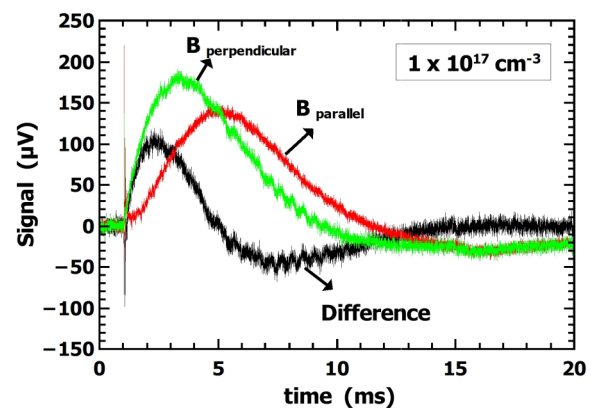


FIG. 8. Measured Hall voltage by subtracting measured parallel data from measured perpendicular data.

Additional measurements were done on the very same samples, whose experimental data are shown in Fig. 6; this time we keep them perpendicular to the field. One such result is shown in Fig. 8. Since V_{bi} (or V_{bi}^*) is not dependent on the sample orientation in the magnetic field, a pure Hall voltage is obtained when the parallel orientation signal is subtracted from the perpendicular one.

We show the experimental data for only one doping density (S1) in Fig. 8, however, the results are very similar for the other three samples (S2–S4).

IX. EXTRACTING THE ITINERANT MAGNETIC SUSCEPTIBILITY

In this section we outline a calculation scheme which highlights how to extract free carrier magnetization (M) or free carrier magnetic susceptibility (χ) from experimental data that give μ vs B . The expressions for M and χ have been stated in Sec. I.

From the experimentally obtained $\mu(B)$ vs B plot, one can find the coefficient γ , assuming a weak-field approximation (which was verified to be valid for our case—see Sec. V A),

$$\mu(B) = \gamma B^2. \quad (11)$$

Before the extraction of γ , the $\mu(B)$ vs B plot must be corrected for any RC effect that is present.

Preliminary calculations yield the expression for χ_{mol} , the molar susceptibility measured in cm^3/mol ,

$$\chi_{\text{mol}} = -\frac{\mu_0 M_w}{2\pi\rho} \gamma N. \quad (12)$$

In Eq. (12), $\mu_0 = 4\pi \times 10^{-7} \text{ H m}^{-1}$ is the magnetic permeability of vacuum, M_w is the molecular mass in g/mol , and ρ is the density in g cm^{-3} . For GaAs, we have $M_w \sim 144.645 \text{ g/mol}$ and $\rho \sim 5.32 \text{ g cm}^{-3}$. γ is measured in J T^{-2} and N in m^{-3} .

For the nondegenerate V_{bi} calculated for n -GaAs at room temperature (see Fig. 3) we have $V_{bi} \sim (4.8 \times 10^{-6} B^2) \text{ V}$, i.e., $\mu \sim q(4.8 \times 10^{-6} B^2) \text{ J}$. Now, from experimentally obtained data (shown in Fig. 6), we calculate the coefficient γ for each of the four doping types of GaAs—including corrections for the sample's individual R_S, C_S after referring to the equivalent

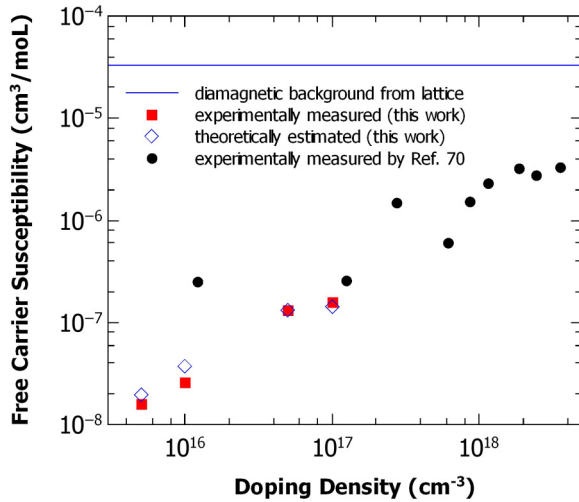


FIG. 9. Absolute magnetic (molar) susceptibilities of the free electrons in n -type GaAs for various doping densities.

circuit of Fig. 4(ii)—and then extract the individual χ_{mol} values from Eq. (12). Results are summarized in Fig. 9.

The theoretical weak-field Landau-Peierls diamagnetic susceptibility, in the nondegenerate limit, is given by (see, for example, Ref. [86])

$$\chi = -\frac{1}{3} \left(\frac{m_0}{m^*} \right)^2 \left[\frac{\mu_B^2 N}{k_B T} \right]. \quad (13)$$

A similar expression derived in the degenerate limit (see, for example, Ref. [87]) has χ varying as $N^{\frac{1}{3}}$ instead.

The diamagnetic background for GaAs is taken directly from Refs. [46,70]. The respective theoretical estimates are calculated from Eq. (13), where N is taken to be the carrier concentration rather than the doping density (the two are different owing to the phenomenon of carrier freeze-out which is non-negligible mostly for the two higher doped samples). For comparison purposes, we also show, in Fig. 9, the itinerant susceptibility data published by Hesjedal *et al.* [70]; these data, reproduced from Fig. 4 of their paper, are in the degenerate limit instead. It is interesting to note how the SQUID saturates

at carrier concentrations lower than 10^{17} cm^{-3} in their work, which clearly shows the advantage of extracting χ using the technique demonstrated in this work.

X. CONCLUSION

We have experimentally detected the magnetic field dependence of the electron chemical potential in n -type GaAs, at room temperature, for four different doping densities. Through a systematic investigation, we have ruled out any spurious voltages, such as the pickup or the Hall voltage from vitiating our experimental data. Our data quantitatively match the expected signal which was calculated from theory. The magnetic field dependence of the electron chemical potential was unambiguously detected for 3D or bulk materials, or at room temperature, since the discovery of the spurious Hall voltage [43] in such experimental trials.

We demonstrate that such experiments could directly yield the fraction of a sample's magnetization that is associated with its itinerant carriers. We extract the Landau-Peierls diamagnetic susceptibility of n -type GaAs, from our measured data, for doping densities as low as 1×10^{16} or $5 \times 10^{15} \text{ cm}^{-3}$. In that light, this is an experimental demonstration of a measurement of magnetic susceptibility as low as $\sim 1 \times 10^{-8} \text{ cm}^3/\text{mol}$, which is $\sim 10^3$ times smaller than the diamagnetic background stemming from the GaAs host lattice, and which is ~ 10 times lower than the measurement sensitivity of the SQUID [70].

This experiment deserves to be tried in systems such as ferromagnetic metals, magnetic semiconductors, or other exotic magnetic systems (such as the hexaborides) to know what fraction of their resulting magnetism is itinerant in nature. Currently there exists an active debate on the origin of ferromagnetism in several such systems.

ACKNOWLEDGMENTS

The Centre for Nano Science and Engineering, IISc, Bangalore is duly acknowledged for providing sample fabrication facilities. Sandip Mondal helped to carry out the ellipsometry measurements. Special thanks to Mr. Karthik of Bright Electronics, Bangalore for the reflow soldering of INA121U on the amplifier PCB.

-
- [1] J. Kubler, *Theory of Itinerant Electron Magnetism* (Oxford University Press, New York, 2009), Chap. 1.
 - [2] T. Dietl, *Nat. Mater.* **9**, 965 (2010).
 - [3] H. Ohno, *Science* **281**, 951 (1998).
 - [4] A. H. Macdonald, P. Schiffer, and N. Samarth, *Nat. Mater.* **4**, 195 (2005).
 - [5] J. Philip, A. Punnoose, B. I. Kim, K. M. Reddy, S. Layne, J. O. Holmes, B. Satpati, P. R. Leclair, T. S. Santos, and J. S. Moodera, *Nat. Mater.* **5**, 298 (2006).
 - [6] H. Ohno, A. Shen, F. Matsukura, A. Oiwa, A. Endo, S. Katsumoto, and Y. Iye, *Appl. Phys. Lett.* **69**, 363 (1996).
 - [7] A. Van Esch, L. Van Bockstal, J. De Boeck, G. Verbanck, A. S. van Steenberghe, P. J. Wellmann, B. Grietens, R. Bogaerts, F. Herlach, and G. Borghs, *Phys. Rev. B* **56**, 13103 (1997).
 - [8] T. Makarova, in *Handbook of Nanophysics: Principles and Methods*, edited by K. D. Sattler (CRC Press, Boca Raton, FL, 2010), Chap. 25.
 - [9] H. Munekata, H. Ohno, S. von Molnar, A. Segmuller, L. L. Chang, and L. Esaki, *Phys. Rev. Lett.* **63**, 1849 (1989).
 - [10] H. Ohno, H. Munekata, S. von Molnar, and L. L. Chang, *J. Appl. Phys.* **69**, 6103 (1991).
 - [11] R. N. Bhatt, M. Berciu, M. P. Kennett, and X. Wan, *J. Supercond. Novel Magn.* **15**, 71 (2002).
 - [12] Y. Zhang and S. Das Sarma, *Phys. Rev. B* **72**, 115317 (2005).
 - [13] F. Bloch, *Z. Phys.* **57**, 545 (1929).
 - [14] E. C. Stoner, *Proc. R. Soc. London, Ser. A* **165**, 372 (1938).
 - [15] E. C. Stoner, *Proc. R. Soc. London, Ser. A* **169**, 339 (1938).

- [16] D. P. Young, D. Hall, M. E. Torelli, Z. Fisk, J. L. Sarrao, J. D. Thompson, H. R. Ott, S. B. Oseroff, R. G. Goodrichk, and R. Zysler, *Nature (London)* **397**, 412 (1999).
- [17] D. Ceperley, *Nature (London)* **397**, 386 (1999).
- [18] M. E. Zhitomirsky, T. M. Rice, and V. I. Anisimov, *Nature (London)* **402**, 251 (1999).
- [19] S. Blundell, *Magnetism in Condensed Matter* (Oxford University Press, New York, 2001).
- [20] O. Prus, Y. Yaish, M. Reznikov, U. Sivan, and V. Pudalov, *Phys. Rev. B* **67**, 205407 (2003).
- [21] M. Reznikov, A. Y. Kuntsevich, N. Tench, and V. M. Pudalov, *JETP Lett.* **92**, 470 (2010).
- [22] V. I. Nizhankovskii and S. G. Zybtev, *Phys. Rev. B* **50**, 1111 (1994).
- [23] W. Thomson, *Philos. Mag.* **46**, 82 (1898).
- [24] D. B. Montgomery, *Solenoid Magnet Design* (Wiley, New York, 1969), Chap. VII.
- [25] $qV_{bi}(B) = \mu(B)$, whereas the corresponding B -dependent change of the gate metal's electron chemical potential $\mu_M(B)$ has been assumed to be negligible. $\mu(B)$'s nonzero offset $\mu(0)$ has also been ignored. q = electronic charge.
- [26] V. M. Pudalov, S. G. Semenchinskii, and V. S. Édel'man, Pis'ma Zh. Eksp. Teor. Fiz. **39**, 474 (1984) [*JETP Lett.* **39**, 576 (1984)].
- [27] V. M. Pudalov, S. G. Semenchinskii, and V. S. Édel'man, Zh. Eksp. Teor. Fiz. **89**, 1870 (1985) [*Sov. Phys. JETP* **62**, 1079 (1985)].
- [28] V. I. Nizhankovskii, B. K. Medvedev, and V. G. Mokerov, Pis'ma Zh. Eksp. Teor. Fiz. **47**, 343 (1988) [*JETP Lett.* **47**, 410 (1988)].
- [29] V. I. Nizhankovskii, V. G. Mokerov, B. K. Medvedev, and Y. V. Shaldin, Zh. Eksp. Teor. Fiz. **90**, 1326 (1986) [*Sov. Phys. JETP* **63**, 776 (1986)].
- [30] D. Weiss, V. Mosser, V. Gudmundsson, R. R. Gerhardt, and K. v. Klitzing, *Solid State Commun.* **62**, 89 (1987).
- [31] R. T. Zeller, F. F. Fang, B. B. Goldberg, S. L. Wright, and P. J. Stiles, *Phys. Rev. B* **33**, 1529 (1986).
- [32] A. M. Dabiran, R. T. Zeller, F. F. Fang, S. L. Wright, and P. J. Stiles, *Surf. Sci.* **196**, 712 (1988).
- [33] R. H. Walmsley, *Phys. Rev. Lett.* **8**, 242 (1962).
- [34] V. I. Nizhankovskii, *Eur. Phys. J. B* **53**, 1 (2006).
- [35] A. D. Caplin and D. Shoenberg, *Phys. Lett.* **18**, 238 (1965).
- [36] W. B. Whitten and A. Piccini, *Phys. Lett.* **20**, 248 (1966).
- [37] N. E. Alekseevskii and V. I. Nizhankovskii, Zh. Eksp. Teor. Fiz. **88**, 1771 (1985) [*Sov. Phys. JETP* **61**, 1051 (1985)].
- [38] B. I. Verkin, L. N. Pelikh, and V. V. Eremenko, Dokl. Akad. Nauk. SSSR **159**, 771 (1964) [*Sov. Phys. Dokl.* **9**, 1076 (1965)].
- [39] L. N. Pelikh, Fiz. Tverd. Tela **8**, 1954 (1966) [*Sov. Phys.-Solid State* **8**, 1550 (1966)].
- [40] V. I. Nizhankovskii, R. N. Sheftal', and S. G. Zybtev, Pis'ma Zh. Eksp. Teor. Fiz. **55**, 242 (1992) [*JETP Lett.* **55**, 238 (1992)].
- [41] H. S. Belson, *J. Appl. Phys.* **37**, 1348 (1966).
- [42] D. Shoenberg, *Magnetic Oscillations in Metals*, Cambridge Monographs on Physics (Cambridge University Press, Cambridge, UK, 1984), pp. 150–153, 477–478.
- [43] M. Peter, D. L. Randles, and D. Shoenberg, *Phys. Lett. A* **33**, 357 (1970).
- [44] M. I. Kaganov, I. M. Lifshitz, and K. D. Sinel'nikov, Zh. Eksp. Teor. Fiz. **32**, 605 (1957) [*Sov. Phys. JETP* **5**, 500 (1957)].
- [45] I. O. Kulik and G. A. Gogadze, Zh. Eksp. Teor. Fiz. **44**, 530 (1963) [*Sov. Phys. JETP* **17**, 361 (1963)].
- [46] S. Hudgens, M. Kastner, and H. Fritzsche, *Phys. Rev. Lett.* **33**, 1552 (1974).
- [47] R. M. Candea, S. J. Hudgens, and M. Kastner, *Phys. Rev. B* **18**, 2733 (1978).
- [48] D. J. Chadi, R. M. White, and W. A. Harrison, *Phys. Rev. Lett.* **35**, 1372 (1975).
- [49] V. P. Sukhatme and P. A. Wolff, *Phys. Rev. Lett.* **35**, 1369 (1975).
- [50] T. Sahu and P. K. Misra, *Phys. Rev. B* **26**, 6795 (1982).
- [51] T. Sahu, *Phys. Rev. B* **43**, 2415 (1991).
- [52] E. Mooser, *Phys. Rev.* **100**, 1589 (1955).
- [53] E. Sonder and H. C. Schweinler, *Phys. Rev.* **117**, 1216 (1960).
- [54] R. N. Bhatt, *Phys. Rev. Lett.* **48**, 707 (1982).
- [55] D. K. Stevens, J. W. Cleland, J. H. Crawford, Jr., and H. C. Schweinler, *Phys. Rev.* **100**, 1084 (1955).
- [56] F. T. Hedgecock, *Can. J. Phys.* **34**, 43 (1956).
- [57] F. T. Hedgecock, *J. Electron* **2**, 513 (1956).
- [58] A. V. Itterbeek and W. Duchateau, *Physica* **22**, 649 (1956).
- [59] R. Bowers, *Phys. Rev.* **108**, 683 (1957).
- [60] D. H. Damon and A. N. Gerritsen, *Phys. Rev.* **127**, 405 (1962).
- [61] E. Sonder and D. K. Stevens, *Phys. Rev.* **110**, 1027 (1958).
- [62] K. Andres, R. N. Bhatt, P. Goalwin, T. M. Rice, and R. E. Walstedt, *Phys. Rev. B* **24**, 244 (1981).
- [63] M. P. Sarachik, D. R. He, W. Li, M. Levy, and J. S. Brooks, *Phys. Rev. B* **31**, 1469 (1985).
- [64] A. Roy, M. Turner, and M. P. Sarachik, *Phys. Rev. B* **37**, 5522 (1988).
- [65] D. K. Stevens and J. H. Crawford, Jr., *Phys. Rev.* **99**, 487 (1955).
- [66] R. Bowers and Y. Yafet, *Phys. Rev.* **115**, 1165 (1959).
- [67] T. Datta, A. Barrientos, J. Amirzadeh, and E. A. Jones, Jr., *J. Appl. Phys.* **61**, 3555 (1987).
- [68] A. Ney, J. S. Harris, Jr., and S. S. P. Parkin, *J. Phys.: Condens. Matter* **18**, 4397 (2006).
- [69] A. Ney, G. Jan, and S. S. Parkin, *J. Appl. Phys.* **99**, 043902 (2006).
- [70] T. Hesjedal, U. Kretzer, and A. Ney, *Semicond. Sci. Technol.* **27**, 055018 (2012).
- [71] G. A. Busch and E. Mooser, *Helv. Phys. Acta* **26**, 611 (1953).
- [72] W. Sasaki and J. Kinoshita, *J. Phys. Soc. Jpn.* **25**, 1622 (1968).
- [73] O. V. S. N. Murthy and V. Venkataraman, *Rev. Sci. Instrum.* **78**, 113905 (2007).
- [74] See Supplemental Material at <http://link.aps.org/supplemental/10.1103/PhysRevB.93.045208> for more details about the experimental setup, sample, and theoretical estimates of some parameters (expected V_{bi} ; fitted C_c , C_{sh} , and R_{sh}).
- [75] P. S. Kireev, *Semiconductor Physics* (MIR, Moscow, 1975), pp. 219–226.
- [76] R. B. Dingle, *Proc. R. Soc. London, Ser. A* **211**, 517 (1952).
- [77] R. E. Peierls, *Z. Phys.* **80**, 763 (1933).
- [78] M. R. Vilar, J. E. Beghdadi, F. Debontridder, R. Artzi, R. Naaman, A. M. Ferrara, and A. M. B. do Rego, *Surf. Interface Anal.* **37**, 673 (2005).
- [79] A. G. Baca, F. Ren, J. C. Zolper, R. D. Briggs, and S. J. Pearton, *Thin Solid Films* **308–309**, 599 (1997).

- [80] E. D. Marshall, S. Zhang, I. C. Wang, P. F. Jiao, W. X. Chen, T. Sawada, S. S. Lau, K. L. Kavanagh, and T. F. Kuech, *J. Appl. Phys.* **62**, 942 (1987).
- [81] J. Lai and J. Y. Lee, *Appl. Phys. Lett.* **64**, 229 (1994).
- [82] N. M. Sawant and R. S. Srinivasa, *J. Appl. Phys.* **75**, 2086 (1994).
- [83] K. Steiner, *IEEE Trans. Instrum. Meas.* **42**, 39 (1993).
- [84] S. Tongay, A. F. Hebard, Y. Hikita, and H. Y. Hwang, *Phys. Rev. B* **80**, 205324 (2009).
- [85] By the phrase “measured signal” we mean the voltage experimentally measured across the resistor R_L , in the magnetic field, after the pickup cancellation has been performed.
- [86] A. H. Wilson, *The Theory of Metals*, 2nd ed. (Cambridge University Press, Cambridge, UK, 1953), pp. 150–153, 175–176.
- [87] L. D. Landau and E. M. Lifshitz, *Statistical Physics, Course of Theoretical Physics*, 3rd ed. (Butterworth-Heinemann/Elsevier, Amsterdam, 2005), Vol. 5, pp. 158–166.